On the Design of Low-Cost Inductive Conductivity Sensors for Salinity Measurement in Oceangoing IoT Applications

Finn J. Klar, Julius Harms, Thorsten A. Kern
Institute for Mechatronics in Mechanics, Hamburg University of Technology, Germany, imek@tuhh.de

Abstract

In this paper, a low-cost transformer type inductive conductivity sensor for the use of in situ measurement of seawater on oceangoing sensor buoys is designed, developed, and tested. The sensor design uses DAC and ADC peripherals of a SAME51 microcontroller. A single PCB holds the MCU, the coils of the transformer type sensor, and circuits for measurement and power supply. The sensor was tested in an ionic solution of increasing conductivity in the range of seawater. The processed readouts from the MCUs ADC sampling at 40 kHz are compared to those sampled by an external oscilloscope of 40 kHz sampling rate, connected to the ADCs inputs. The processed ADC data show a significantly higher sensor gain and sensor gain slope compared to the oscilloscope data. The influence of high-frequency noise in combination with the lower sampling rate is considered a possible cause. The measurement results show that a revision of the amplifier circuit, the target offset voltage, and the amplifier loop gain is necessary.

1 Introduction

Inductive conductivity sensors have the advantage of allowing a protective housing that prevents biofouling and corrosion. In contrast, conductivity cells require more maintenance but stand out due to a lower purchase price. Conductivity cells are commonly used in low-cost applications, even though inductive sensors would offer clear advantages in the long run. In addition, most conductivity sensors on the market are designed for industrial applications and come with large transducers. Especially in IoT applications, there is often a need for compact and cost-effective sensors that provide simple data interfaces.

The authors of this paper are developing a low-cost, oceangoing sensor buoy that enables high spatial resolution measurement for in situ ocean monitoring [1]. Here, a cost-efficient but reliable water conductivity measurement for salinity determination poses one of the biggest challenges. A previous study examined the measurement uncertainties of an transformer type inductive conductivity sensor (TICS) using a low-cost approach [2]. Dankert et al. [3] introduced the theory of an TICS in 1985 and derived an equivalent circuit still used today. Authors have examined [4, 5, 6] the performance of TICS in the industrial field and provided approaches for reducing implementation costs.

In the following, an implementation of a low-cost TICS for the measurement of seawater conductivity based on a simple integrated circuit is proposed. Different approaches for the measurement concept are discussed and compared based on simulations of the equivalent model representation. A measurement circuit and the exact sensor coil parameters are selected and implemented on a single PCB. Finally, the resolution of the sensor is validated using different conductive solutions.

2 Sensor Concept

The sensor consists of two coaxial aligned coils of toroid shape. A current passing through the primary coil creates a magnetic flux in the coil core. This flux passes though the water loop, surrounding the toroid. This leads to an ionic current in the water, creating magnetic fluxes in the primary and secondary ferrite cores, thus generating a current in the secondary coil. The physical sensor concept can be represented by the equivalent circuit shown in **Figure 1a**, which is based on the TICS introduced by Dankert et al. [3].

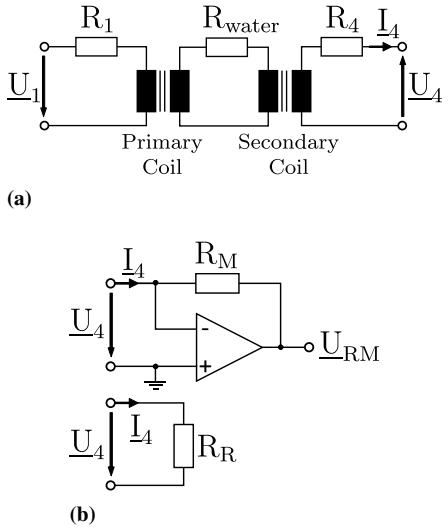

Figure 1 a: Equivalent model representation of TICS by Dankert et al. [3]. b: Short Circuit measurement by virtual ground concept (top) and high impedance termination for open circuit measurement (button).

The equations describing the currents and voltages of the equivalent circuit were illustrated by Hui et al. [4]. They

ISBN 978-3-8007-5835-7

determined the governing equations for each section to be

$$I_1 = \frac{A}{A\,(R_1 + jL_1\omega) + M_{12}^2\omega^2} U_1, \tag{1}$$

$$I_2 = -\frac{jM_{12}\omega}{A} I_1, \tag{2}$$

$$I_4 = -\frac{jM_{34}\omega}{R_R + R_4 + jL_4\omega} I_2 \tag{3}$$

and

$$A = \frac{M_{34}^2\omega^2}{R_R + R_4 + jL_4\omega} + (R_W + jL_2\omega + jL_3\omega). \tag{4}$$

The equations 1 to 4 are used to model sensor behavior in MATLAB and simulink to investigate the effect of sensor parameters such as coil windings, core permeability, excitation and sampling to enable the determination of seawater salinity by measuring conductivity. As a requirement, the measurement range for seawater is chosen between 2 mS/cm and 75 mS/cm with temperature changes between 0 °C and 30 °C. The minimum required measurement resolution is derived from the aimed salinity accuracy of 0.05 psu, which corresponds to 0.0345 mS/cm in the lower temperature range. This translates to 460 ppm of the upper bound of the targeted conductivity range.

Based on the model representation, different excitation concepts are investigated using a simulation. **Figure 2** compares an open circuit with a virtual short circuit measurement as proposed by Hui et al. [4].

The virtual short circuit is implemented with a transimpedance converter and for the open circuit measurement a voltage is measured across a high impedance terminating resistor (**Figure 1b**). The mutual coupling factor is modeled to 0.99, the permeability is modeled according to the properties of the ferrite N87 by TDK. Its initial permeability is 1888 for 0 °C, 2200 for 20 °C and 2658 for 40 °C. The resistance of the measuring amplifier circuit R_M is modeled to be 1 Ω.

Figure 2 shows that in the open circuit measurement, the sensor gain is larger and the sensitivity to the measurand is higher, but at the same time, it is nonlinear and more susceptible to changes in permeability μ_R. Using a current source to attenuate the sensor neglects the effect of temperature on the primary coil current. **Figure 3** shows the sensor output for this setup. This configuration performs similar to the open circuit, voltage-driven system.

To minimize the influence of disturbances, the virtual ground circuit with linear characteristics is chosen for implementation. Hui et al. [4] argued to choose magnetic cores of high permeability to match simplifications used in their model. As these simplifications do not apply for our model, based on the equations 1 to 4, the added value of high permeability cores is to be investigated. **Figure 4** compares the sensor gain for cores of different permeability under the precondition of a coupling factor of 0.99. The figure suggests better sensor performance for ferrite of low permeable ferrite. Thus a toroidal ferrite of low permeability is chosen, this is N87 by TDK due to good availability.

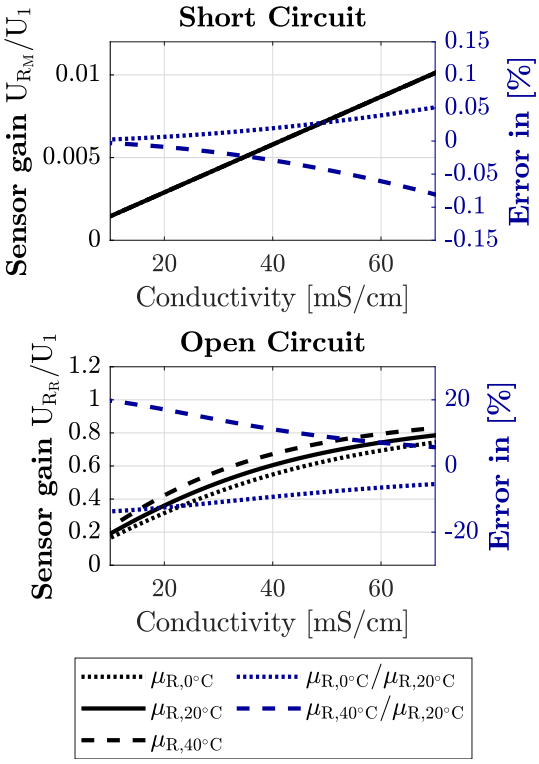

Figure 2 Simulation results of the sensor gain for the concepts of short circuit and open circuit measurement. Displayed is the sensor gain in terms of the voltage input output ratio for different relative permeability's μ_R resulting from different core temperatures and the relative error related to the value at 20°C.

Figure 5 shows the integrated sensor concept in a block diagram. The internal ADCs and DACs of the CAN-enabled microcontroller SAME51 are used to excite and sample the sensor signals. The ADCs are configured in differential mode, using the analog ground as the second input source. A REF4132-Q1 device generates the reference voltage of 2.5 V used by ADCs and DACs. A differential amplifier is used to generate an oscillating signal centered at 0 V. The coils are designed for a sinusoidal attenuation with 1 V amplitude. The winding count is set to 26, decreasing the secondary coil current below a 10 mA threshold. **Table 1** contains the design parameters of used coils and cores.

Table 1 Parameters of coils and cores.

Parameter name	Value
Core material	N87
Core permeability, μ_i	2,200 ±25%
Winding primary coil	26
Winding secondary coil	26
Radius of copper wire	0.3 mm
Core inner diameter	13.5 mm
Core outer diameter	26.6 mm
Core height	11 mm

The circuit is built on a single PCB, which reduces the size

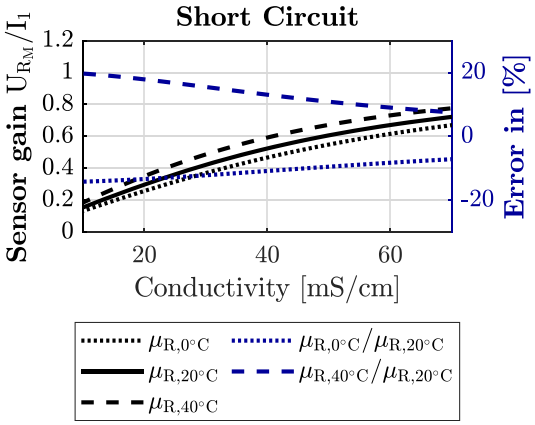

Figure 3 Simulated sensor gain for the concept using a short circuit and a current source.

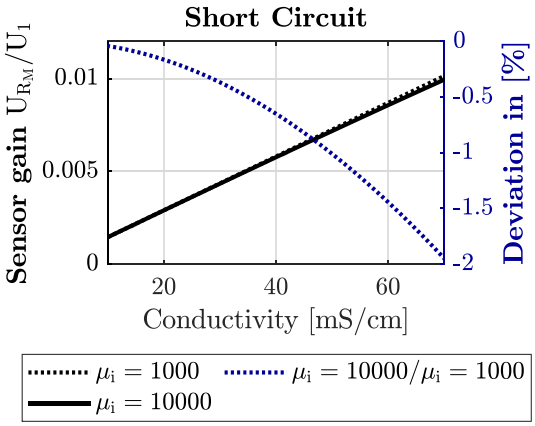

Figure 4 Influence of core permeability on sensor gain.

of the sensor and the manufacturing costs. The toroidal coils are mounted on the top and bottom of the PCB and shielded from each other with a copper ring to reduce stray couplings. After assembly, the sensor circuit is encapsulated in PU resin.

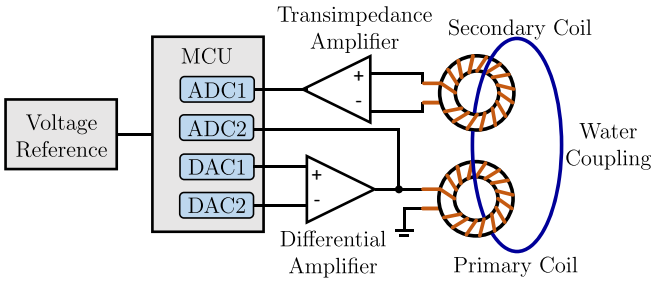

Figure 5 Simplified block diagram of integrated sensor circuit.

3 Implementation and Test

For a test, the described sensor concept is implemented as shown in **Figure 6**. This setup uses an amplifier feedback resistor R_M of 600 Ω. An offset voltage of 830 mV is measured between ground and ADC input on the secondary side. Post assembly, coaxial cables were soldered to vias connected to analog ground, ADC, and DAC for monitoring sensor behavior. A 3D model of the housing is printed to create a negative mold for casting. The sensor circuit is placed on a carrier, centering the PCB in the mold. Model, mold, and PU encapsulated sensor are displayed in **Figure 7**. The size of the housing is 90.16 x 68.3 x 30.4 mm^3, following the outline of the PCB with an offset of 2 mm. The inductance of the implemented coils is measured to 1.7 mH and the effect of the PCB isolation on the stray inductance is investigated. LCR readings on setups with and without shielding (**Figure 8**) show effects at the resonance frequency. The differences around the desired attenuation of 10 kHz are 29.6 nH at 9.8 kHz and 27.7 nH at 10.1 kHz.

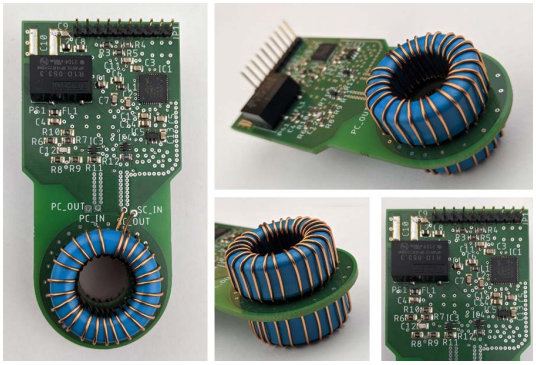

Figure 6 Photos of the implemented sensor circuit prior to cast molding in resin.

Figure 7 Photo of the 3D printed sensor housing (purple), the silicon based casting mold and the sensor inside the housing.

The PCB is powered by a regulated 5 V source. The MCU is configured to operate with the internal digital frequency control loop at 48 MHz. The peripherals are configured for synchronous operation. A sequence of one DAC write command and two ADC read commands is repeated to generate the attenuation voltage and sample the TICS input and output voltage. Evaluation of the propagation time of the sequences shows real-time capability for up to 50 kHz, allowing quantization of the desired 10 kHz signal to up to five quantiles. The quantization of the sine wave into four sections allows sampling of the peaks and

ISBN 978-3-8007-5835-7

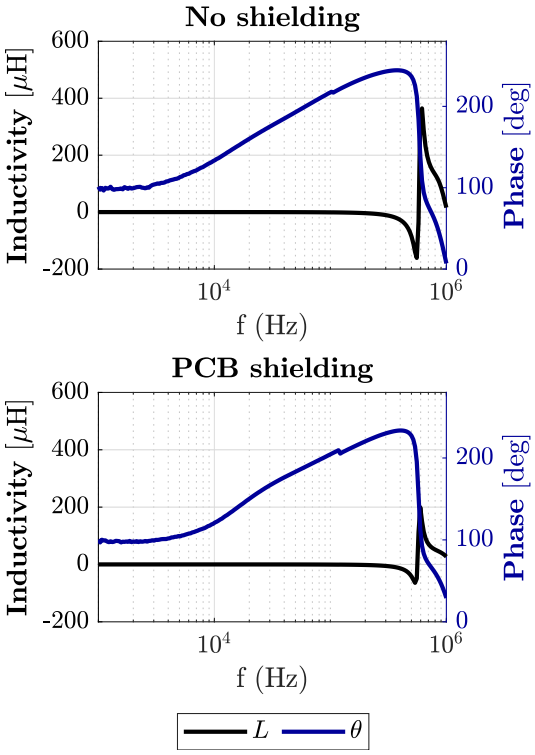

Figure 8 LCR reading of TICS setup without and with shielding showing the mutual inductance between primary and secondary coil M_{14}.

zeros. An oscilloscope sampling at 10 MHz is connected to the ADC inputs via the coaxial cables to evaluate the additional value of higher sampling rates. At the same time, a function generator is connected to the DAC pins to determine the influence of a high-resolution sine wave. The sampled data points are evaluated on a computer using an FFT. By dividing the 10 kHz amplitude from the frequency range of the recorded voltage curve of U_{R_M} (ADC1) by that of U_1 (ADC2), the sensor gain for the respective measuring point is determined. The sensor is immersed in purified water to which salt is added, changing the conductivity value of the water. The water is stirred until the salt is dissolved. Data points are collected as soon as the reference conductivity sensor outputs constant values with a resolution of one decimal point. The DAC-driven test is conducted first, followed up by an attenuation using the external function generator. The evaluated test results are displayed in **Figure 9**. The sensor response is of a linear characteristic. The maximum sensor gain is achieved for the signal sampled by the MCU. The calculated gain rises from 39.5812 for 10.9 psu to 57.584 for 73.8 psu, which equals 0.302 psu^{-1}. The gain on the oscilloscope reads are 0.1687 psu^{-1} for DAC attenuated test and 0.1722 psu^{-1} for the attenuation using the function generator. The difference in offset and slope can be a result of noise disturbing the ADC samples. According to the Nyquist theorem, only signals of frequencies up to half the sampled frequency can be reconstructed from the samples. The ADC peripherals sampling data at 40 kHz allow for signal components of frequencies above 20 kHz to disturb unnoticed.

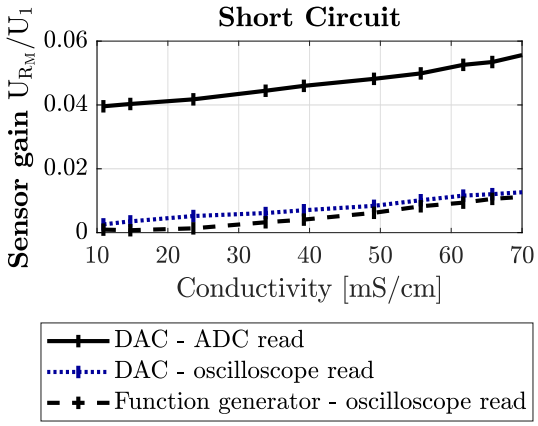

Figure 9 Evaluated measurement data.

4 Results and Conclusion

In this work, a low-cost and compact inductive conductivity sensor has been designed, developed, and tested. The sensor is based on a TICS design and implemented on an integrated circuit with a CAN-enabled microcontroller. The results of the experiments performed show promising sensor characteristic. Future work should be carried out to improve the analogue circuit as the sum of measured voltage offset and evaluated measurement data is below the reference voltage of 2.5 V at the upper end of the suggested conductivity spectrum. The analysis of the log time stability and a detailed analysis of achievable resolution is to be investigated. The impact of an off grid DC power source for the chip is of additional interest.

5 References

[1] J. Harms and T. A. Kern. Proof of concept validation of a swimming multi sensor platform for in-situ ocean monitoring. In *SMSI 2021 - Sensors and Instrumentation*. AMA Service GmbH, Von-Münchhausen-Str. 49, 31515 Wunstorf, Germany, 2021. doi: 10.5162/smsi2021/b4.4.

[2] Y. Kandur, J. Harms, and T. A. Kern. Uncertainty analysis for low-cost transformer-type inductive conductivity sensors. *Engineering Proceedings*, 6(1), 2021. doi: 10.3390/I3S2021Dresden-10145.

[3] K. Striggow and R. Dankert. The exact theory of inductive conductivity sensors for oceanographic application. *IEEE Journal of Oceanic Engineering*, 10 (2):175–179, 1985. doi: 10.1109/JOE.1985.1145085.

[4] S. Kang Hui, Jang H., Kim Gum C., Yu Song C., and Kim Yong H. A new design of inductive conductivity sensor for measuring electrolyte concentration in industrial field. *Sensors and Actuators A: Physical*, 301:111761, 2020. doi: 10.1016/j.sna.2019.111761.

[5] R. T. Wood, A. Bannazadeh, N. Q. Nguyen, and L. G. Bushnell. A salinity sensor for long-term data collection in estuary studies. In *OCEANS 2010 MTS/IEEE SEATTLE*, pages 1–6, 2010. doi: 10.1109/OCEANS.2010.5664602.

[6] S. Wu, H. Lan, J. Liang, Y. Tian, Y. Deng, H. Li, and N. Liu. Investigation of the performance of an inductive seawater conductivity sensor. *Sensors & Transducers*, 186(3):43–48, 2015.